

Sensitivity of Biomarkers to Changes in
Chemical Emissions in the Earth's Proterozoic Atmosphere

Grenfell, J.L.¹, Gebauer, S.¹, von Paris, P.², Godolt, M.¹,
Hedelt, P.^{2*}, Patzer, A.B.C.¹, Stracke, B.², and Rauer, H.^{1,2}

(1) Zentrum für Astronomie und Astrophysik (ZAA)

Technische Universität Berlin (TUB)

Hardenbergstr. 36

10623 Berlin

Germany

(2) Institut für Planetenforschung (PF)

Deutsches Zentrum für Luft- und Raumfahrt (DLR)

Rutherford Str. 2

12489 Berlin

Germany

*Now at :

Laboratoire d'Astrophysique de Bordeaux (LAB)

Université de Bordeaux – CNRS

BP 89

33271 Floirac cedex

France

27 Pages, 5 Figures, 4 Tables.

Running Head: Atmosphere, Proterozoic, Biomarker

Editorial correspondence and proofs to:

Dr. John Lee Grenfell

Zentrum für Astronomie und Astrophysik (ZAA)

Technische Universität Berlin (TUB)

Hardenbergstr. 36

10623 Berlin

Germany

Email: lee.grenfell@dlr.de

Abstract: The search for life beyond the Solar System is a major activity in exoplanet science. However, even if an Earth-like planet were to be found, it is unlikely to be at a similar stage of evolution as the modern Earth. It is therefore of interest to investigate the sensitivity of biomarker signals for life as we know it for an Earth-like planet but at earlier stages of evolution. Here, we assess biomarkers i.e. species almost exclusively associated with life, in present-day and in 10% present atmospheric level oxygen atmospheres corresponding to the Earth's Proterozoic period. We investigate the impact of proposed enhanced microbial emissions of the biomarker nitrous oxide, which photolyses to form nitrogen oxides which can destroy the biomarker ozone. A major result of our work is regardless of the microbial activity producing nitrous oxide in the early anoxic ocean, a certain minimum ozone column can be expected to persist in Proterozoic-type atmospheres due to a stabilising feedback loop between ozone, nitrous oxide and the ultraviolet radiation field. Atmospheric nitrous oxide columns were enhanced by a factor of 51 for the Proterozoic "Canfield ocean" scenario with 100 times increased nitrous oxide surface emissions. In such a scenario nitrous oxide displays prominent spectral features, so may be more important as a biomarker than previously considered in such cases. The run with "Canfield ocean" nitrous oxide emissions enhanced by a factor of 100 also featured additional surface warming of 3.5K. Our results suggest that the Proterozoic ozone layer mostly survives the changes in composition which implies that it is indeed a good atmospheric biomarker.

Key words: atmospheres, Proterozoic, photochemistry, biomarkers.

1. Introduction

Investigating atmospheric spectral signatures of species which potentially indicate life (biomarkers) on terrestrial exoplanets may be an attainable goal in the not-too-distant future. A central motivation is to assess how robust such signals are under varying atmospheric conditions and to differentiate signatures of life from the so-called “false positives” which mimic life. Stars in the solar neighborhood are mainly young (e.g. Lopez-Santiago et al., 2004) hence, if they possess terrestrial planets, their age is expected to be comparable to the Archaean/Proterozoic periods in Earth’s history assuming a similar evolution. Earlier works have assessed the responses of biomarker abundances in low oxygen (O₂) Earth-like atmospheres (Segura et al., 2003). By extending our results to exoplanets in their Habitable Zones (HZs), our approach considers planetary conditions with a similar history, photochemistry, biospheric input and development as in Early Earth’s history.

Ozone (O₃) is considered to be a good biomarker for an Earth-like planet in the HZ because it is mostly formed from biogenic O₂ and it persists in the atmosphere even at very low O₂ levels (Kasting and Donahue, 1980; Segura et al., 2003). Previous studies have discussed the rise in atmospheric O₂ at the start of the Proterozoic (e.g. Catling 2005; Catling and Claire, 2005; Kump et al., 2001) representing their system as boxes (atmosphere, ocean, mantle etc.) interlinked with parameterised expressions for material fluxes. There are however some studies which applied coupled climate-photochemical column models. Some studies (e.g. Schindler and Kasting, 2000; Kaltenecker et al., 2007) presented theoretical spectra spanning the Archaean to the Proterozoic. O₃ is rapidly removed via catalytic cycles involving oxides of e.g. nitrogen (NO_x), chlorine (ClO_x), and hydrogen (HO_x) (Crutzen, 1970; World Meteorological Organization, 1995). The Proterozoic Earth likely featured enhanced volcanic and lightning emissions (Navarro-Gonzalez et al., 1998; Mvondo et al., 2001) which delivered NO_x into the atmosphere hence influenced the presence of O₃. **During the Proterozoic, NO_x recycling (i.e. conversion into its**

main atmospheric reservoir, nitric acid (HNO₃) and back again) may have been faster than today due to stronger solar UV fluxes, which stimulates both HNO₃ production via NO₂+OH+M→HNO₃+M, as well as photolytic loss of HNO₃ back into NO_x. Detailed modelling is thus required to address the non-linear photochemical responses of O₃ to these atmospheric conditions.

Concentrations of methane (Pavlov et al., 2003) and molecular hydrogen (Tian et al., 2005; Catling, 2006) - which can affect not only temperature, but also influence the abundance of HO_x hence (via established catalytic cycles) the biomarker O₃ - were probably higher in the Proterozoic than today. Consequently, another important aspect of investigation is how such changes impact the significance of O₃ as a biomarker. In a baseline study, Segura et al. (2003) investigated O₃ responses to lowering abundances of O₂ using fixed, modern-day concentrations of the long-term source gases: H₂, CO, CH₃Cl, and N₂O at the surface. Our work builds on their study by additionally varying surface-emitted species under Proterozoic Earth conditions, i.e. with low O₂ abundances and a faint young Sun with reduced solar luminosity based on Gough (1981) as discussed e.g. in Ribas et al. (2005). Some of our imposed composition increases (e.g. a doubling in the methane flux) are rather moderate compared with some estimates for the Proterozoic (e.g. Pavlov et al., 2003) but are nevertheless within the uncertainty range and remain within conditions for which our model has been validated.

Another biomarker molecule, nitrous oxide (N₂O) is usually associated almost exclusively with microbial life on the Earth. However, spectral measurements are challenging due to weak and narrow absorption bands for modern atmospheric concentrations. In the Proterozoic period, emissions of N₂O were probably higher than today (Buick, 2007) associated with strong microbial activity in the early anoxic ocean (the so-called “Canfield ocean”), but, on the other hand, possible UV feedbacks may have led to faster N₂O removal via photolysis. Des Marais et al. (2002) and Traub and Jucks (2000) discuss the effect of increased N₂O concentrations upon its spectral signature. Note that (unlike O₃) N₂O is located mostly in the troposphere.

We investigate photochemical feedbacks between the two important biomarkers O₃ and

N₂O using a coupled radiative-photochemical model. Finally, we quantify differences in the spectral signatures (especially for O₃ and N₂O) between the modern Earth and its Proterozoic period by calculating theoretical line-by-line spectra based on the calculated model atmospheres.

2. About the Models and the Runs

2.1 Atmospheric convective-radiative-photochemical column model

The original 1D model is described in detail in Kasting et al. (1984), Segura et al. (2003), Grenfell et al. (2007)^a. The model calculates chemical concentrations and temperature profiles from the planetary surface up to the lower mesosphere. Latest improvements in the model version used here are described in Rauer et al. (2010). The radiative part of the climate module uses a longwave radiation scheme, the Rapid Radiative Transfer Model (RRTM) based on Mlawer et al. (1997) and a shortwave code based on Toon et al. (1989) and Pavlov et al. (2000). Convective adjustment in the troposphere is based on either a moist or dry adiabat depending on whether the saturation pressure of water is exceeded (Ingersoll, 1969). The model employs the relative humidity distribution described in Manabe and Wetherald (1967). The chemistry scheme features 55 species with **212** reactions including the HO_x, NO_x, and ClO_x families. Natural biogenic and source gas emissions were included.

The model calculates global-mean conditions. Oxidation of higher hydrocarbons (C_xH_y) was neglected for $x \geq 2$. Interactive biogeochemical cycles are neglected. To account for missing clouds, the surface albedo in the climate and chemistry modules was adjusted until the converged surface temperature, T₀, reaches the measured mean Earth value of 288.0 K. Clouds influence atmospheric spectra as suggested by Kaltenecker et al. (2007), who showed theoretical spectra for Earth-like atmospheres at various stages of development. Climatic effects of different cloud layers on e.g. T₀ are described elsewhere (Kitzmann et al., 2010) using a version of our model without chemistry. Combining the effect of clouds with atmospheric chemistry is a future task not

included here.

Sulphur compounds may have had an important impact on the redox properties of the atmosphere during the Proterozoic (e.g. Kasting et al., 1989). Sulphur chemistry in the current model version is comparable to Segura et al. (2003) involving 16 sulphur-containing species participating in 62 sulphur reactions. Like the Segura study, we assumed SO₂ and H₂S surface emissions of 58 and 3.3 Tg sulphur per year respectively.

In the modern Earth control run 1, surface emissions were adjusted to reproduce modern day ambient concentrations, an approach already adopted e.g. in Segura et al. (2003) and Grenfell et al. (2007)^{a,b}. Table 1 shows the resulting fluxes adopted in the model. Differences between modelled and observed values in Table 1 are attributed to some missing physical processes e.g. microphysics, and missing chemical reactions in the model. Also, a global average model is not able to include the effects of e.g. non-linear latitudinal variations in chemistry and dynamics. Overall, however, Table 1 suggests a good correspondence of our model fluxes to observations.

Furthermore, in this work we employ the widely-used assumption that atmospheric O₂ forms an isoprofile – even in the case of low O₂ content at 10% Present Atmospheric Levels (PAL). We have confirmed this assumption by comparison with interactive O₂ calculations – further details will be provided by Gebauer et al. (in preparation).

2.2 Theoretical spectra model – output from the atmospheric model (temperature, concentration profiles) is passed as input into the radiative transfer spectral model, SQuIRRL (Schwarzschild Quadrature InfraRed Radiation Line-by-line, Schreier and Böttger, 2003). SQuIRRL is a line-by-line radiative transfer model, which uses molecular absorption line databases (like HITRAN or GEISA) for the calculation of absorption cross-sections and, optionally, continuum absorption corrections. Local thermodynamic equilibrium (LTE) is assumed. Using the absorption cross-sections from HITRAN 2004 (Rothman et al., 2005), SQuIRRL calculates the emission and absorption for a chosen line-of-sight through the atmosphere. A Planck function with the appropriate temperature of the model layer is used as an emission source. The absorption within

the beam is calculated from the surface to a height of ~70 km, divided into approximately 1 km layers as in the photochemical part of the atmospheric column model. The atmosphere is assumed to be cloud and haze free without scattering, consistent with the treatment used in the atmospheric model applied in our work. The emission spectra are calculated using a pencil beam looking down on the atmosphere at a **viewing** angle of 38 degrees as adopted in the previous study of Segura et al. (2003).

Other spectral models in the literature (Selsis et al., 2002; Meadows and Crisp, 1996) comprise high-resolution ($\sim 1\text{cm}^{-1}$ or better) line-by-line codes. The Selsis et al. scheme is based on MODTRAN. SQuIRRL has participated in an intercomparison (Melsheimer et al. 2005) of eight radiative transfer schemes, which suggested deviations of $<10\%$ for the major absorbers between the various models.

2.3 About the runs

2.3.1 Modern Earth control run

The modern Earth control run (run 1, Tables 1, 2) features adjusted surface emissions and an adjusted surface albedo set to 0.21, to reproduce modern-day conditions. The converged model calculated a surface temperature, $T_0=288.0\text{K}$, corresponding to the measured modern Earth mean value with surface concentrations: $\text{CH}_4=1.6\times 10^{-6}$, $\text{H}_2=5.5\times 10^{-7}$, $\text{CO}=9\times 10^{-8}$, $\text{N}_2\text{O}=3\times 10^{-7}$ and $\text{CH}_3\text{Cl}=5\times 10^{-10}$ volume mixing ratio (vmr), which correspond to the modern day (1990) atmosphere. With these values, our model calculated an O_3 column of 305 Dobson Units (DU) ($1\text{DU} = 2.7\times 10^{16}$ molecules cm^{-2}) comparable to observations of $\sim 310\text{DU}$ (IPCC TAR 2007).

2.3.2 Proterozoic low level O_2 Conditions (10% PAL)

In general, O_3 is subject to a “self-repair” mechanism, whereby an initial lowering in O_3

leads to enhanced UV on lower atmospheric levels, which in turn photolyses more O₂, *creating* O₃. Further, an increase in surface emissions of N₂O and CH₃Cl, is expected to release NO_x and ClO_x respectively into the stratosphere, which would likely lead to more O₃ *destruction* via the established catalytic cycles. On the other hand, more NO_x in the troposphere (e.g. from enhanced lightning on the Early Earth) can lead to tropospheric O₃ *production* via the well-known smog mechanism (Haagen-Smit, 1951).

Increasing CH₄ – which may have been an important greenhouse gas during the Proterozoic (Pavlov et al. 2003) - is expected to cool the stratosphere hence can favour O₃ *production* due to a well-known temperature-dependent response in the Chapman cycle, via a slowing in the O₃ sink: $O + O_3 \rightarrow 2O_2$. Also, CH₄ strongly impacts HO_x photochemistry (hence O₃): in the troposphere CH₄ is an important sink for OH, whereas in the stratosphere CH₄ can favour HO_x production since it is oxidised to water, which photolyses into HO_x.

To investigate separately such complex mechanisms, we performed six runs corresponding to the Earth's Proterozoic period (runs 2 to 7, Table 2) with varying composition and having 0.943 times the modern incoming solar flux based on Gough (1981) which corresponds to conditions of about 0.7 Gyrs ago. Generally, where observational evidence is unclear (e.g. for CH₃Cl) rather moderate changes in composition were adopted in this work, so as not to be too far removed from an Earth-like composition where the model has been extensively tested. High N₂O scenarios, were however, also performed, because there are indications of high emissions (Buick 2007) of this specie during the Proterozoic. Our chosen methane surface flux of two times the modern methane fluxes is based approximately on the study of Pavlov et al. (2003) who suggested an increased CH₄ flux by up to a factor ten times the modern value. Emissions of other species for the Proterozoic period were varied as shown in Table 1 as a sensitivity study. CO₂ was lowered to a pre-industrial concentration of 2.77×10^{-4} vmr (IPCC Third Assessment Report (TAR), 2007). Start values of remaining long-lived gases were set to modern levels.

In summary, run 2 represents the Proterozoic control calculation (i.e. the same surface gas emissions as the modern Earth control run 1, but with 10% PAL O₂ and reduced solar luminosity).

Run 3 is as for run 2 but employed increased NO emissions from lightning by a factor of 10 (Navarro-Gonzalez et al., 1998; Mvondo et al., 2001). Run 4 adopts a 100 times increase in surface N₂O emissions, based on the “Canfield” (anoxic) ocean scenario as discussed e.g. in Buick (2007). Run 5 adopts a doubling in CH₄ emissions (Pavlov et al., 2003). Run 6 features a 10-fold increase in CH₃Cl surface emissions, which are rather uncertain for the modern Earth (Keppler et al., 2005). For run 7, H₂ surface fluxes were modified to +25Tg/year, assuming a higher H₂ outgassing rate during the Proterozoic era (Tian et al., 2005), compared with modern Earth conditions (having -5.5 H₂ Tg/year, where the minus sign denotes *loss* on the surface via deposition). **In runs (1-6) we adopted a constant dry deposition velocity for H₂ removal of $7.7 \times 10^{-4} \text{ cm s}^{-1}$. In run 7 we adopted a constant, upwards H₂ flux.** The input parameters of all model runs are summarized in Table 2.

3. Results

Table 3 summarises column values in DU. Figures 1a and 1b show atmospheric profiles of the biomarkers O₃ and N₂O respectively.

3.1 Ozone as a Proterozoic Biomarker

Proterozoic control - for the 10% PAL O₂ run 2 (Table 3), the resulting O₃ column is reduced by 36DU compared with the modern Earth value obtained in run 1, but it is still able to function as an important UV shield. For the 10% PAL O₂ runs, the O₃ peak profile (Figure 1a) is shifted downwards compared with the modern Earth profile run due to the well-known O₃ repair mechanism, as already described above **which led to a strong lowering in O₃ in the mid to upper stratosphere for the Proterozoic control run 2 compared with the modern day control run 1.** Like our work, Segura et al. (2003) also obtained similar O₃ values for their 10% PAL O₂, noting that the O₃ column remained quite robust to a lowering in O₂.

Varying chemical composition – only a small effect upon O_3 arose from increasing CH_4 (run 5, Figure 1a) and H_2 (run 7), since these two lines overlay the 10% PAL O_2 control (run 2) up to about 30km. Increasing N_2O (run 4), which decomposes in the stratosphere to form NO_x , led to strong local O_3 loss in the lower stratosphere with a 32% reduction in the column compared to the Proterozoic control run 2 (see Table 3) due to the established NO_x catalytic chemistry (Crutzen, 1970). Similarly, increasing CH_3Cl (run 6), which photolyses to form ClO_x , also led to significant O_3 loss, but in the mid to upper stratosphere where the ClO_x cycles are favoured and to a 41% reduction in the column compared with run 2 (Table 3). Increasing lightning (run 3) which leads to enhanced NO_x in the troposphere (Figure 1a) resulted in enhanced O_3 here due to production from the smog mechanism (Haagen-Smit, 1951), leading to a 7% increase in the column value compared with run 2. This supports the findings of Grenfell et al. (2006), who proposed that the smog mechanism could play an important role on the Early Earth.

3.2 Nitrous Oxide as a Proterozoic Biomarker

The results listed in Table 3 suggest a strong lowering in the N_2O column (77 DU) in the Proterozoic reference run 2 compared with the modern day control result (233 DU). **Related to this response is the previously-mentioned strong reduction in O_3 in the mid to upper stratosphere since the associated increase in UV implied a stronger sink for N_2O .** To investigate the N_2O response Table 4 summarises the main N_2O atmospheric sinks in the stratosphere at 20km. Note that the atmospheric inorganic sources are negligibly slow and are therefore neglected. Table 4 suggests that the lower N_2O abundances for the Proterozoic reference run 2 are associated with an increased photolytic loss rate compared with run 1.

Comparing run 2 with run 4 in Figure 1 b and Table 3, indicates that increasing the N_2O flux by a factor of one hundred (run 4) leads to an increase in the atmospheric column density of N_2O by a factor of about fifty-one. Thus, the enhanced molecular flux is not completely converted

into a concentration increase of N₂O e.g. because the higher UV in the early Earth's upper stratosphere favoured more photolytic loss as already discussed.

3.2.1 N₂O and O₃ feedback – enhanced N₂O surface fluxes, possibly associated with the Canfield ocean, imply increased NO_x, which is the product of N₂O decomposition in the stratosphere. This reduces O₃ hence increases UV, implying a stronger N₂O photolytic sink, opposing the original increase in N₂O and acting as a negative feedback, as previously mentioned. To investigate this feedback in more detail, we performed a family of “Canfield Ocean Runs” (COR), all having similar conditions to run 4 but with varying N₂O surface emissions by factors, e.g. F = 1, 10, 50, 100, 500, 1000 and 10,000 relative to the modern Earth value. **To validate these high N₂O levels in our RRTM climate scheme, we performed a detailed comparison of RRTM with the line-by-line model SQuIRRL (as described in 2.2) comparing infra-red fluxes at the top of the atmosphere. For F=500 the radiance fluxes in the relatively strong N₂O absorbing bands between 10 and 25 microns agreed to within about 5%. Agreement was weaker at 4-5 microns where the two schemes differed by up to about 30% but absorption in this spectral range was overall very weak. The total integrated radiation fluxes differed by 1.4% (F=500) and 4.2% (F=10,000).**

Figure 2a summarises results for the Canfield Ocean runs. The continuous line shows the increase in atmospheric N₂O column with increasing surface emissions. The short arrowed-feature shows the gradient of the line arising from the three runs with F=1, 10 and 50. Deviation away from this gradient at higher emissions implies a non-linear feedback between N₂O surface emissions and its atmospheric concentration. Increasing emissions led to enhanced NO_x (e.g. from 2.2×10^{-10} vmr (F=1) up to 7.3×10^{-8} vmr (F=1000) in the lower stratosphere at ~20km). This implies a lowering in the O₃ column (Figure 2a), therefore an increase in UV-B, hence a stronger N₂O photolytic sink. Therefore, N₂O concentrations in Figure 2a did not increase linearly with surface emissions. Interestingly, at high N₂O surface emissions, the O₃ column converged - to a value of about 132 DU. In this regime, investigations imply that any further lowering in O₃, led to

an increase in O₂ photolysis (via Chapman production), which balanced the catalytic loss from NO_x. Figure 2b shows the contribution of the Chapman- and smog-mechanisms to the O₃ production near 10km. Results suggest that Chapman is the dominant mechanism, although at very high N₂O surface emissions, the smog mechanism catalysed by NO_x could become significant. **To test whether the mechanism could operate with enhanced chlorine we repeated the F=500 and F=1000 cases with ten times enhanced surface natural CH₃Cl emissions; we found that the effect upon O₃ was insignificant, suggesting that our proposed N₂O-O₃ coupled mechanism was still operating.**

Consequently our result implies that regardless of the level of microbial activity producing N₂O in the early anoxic ocean, which is not well-determined, a certain minimum O₃ column can nevertheless be expected to persist in Proterozoic-type atmospheres due to a stabilising feedback loop between the two biomarker molecules O₃, N₂O and the UV radiation field.

3.3 Methane (CH₄) abundance and temperature responses

3.3.1 CH₄ abundance - Figure 3a implies that increasing the CH₄ surface flux by a factor of 2 in run 5 compared with run 2 leads to an increase by a factor of 2.4 in surface CH₄ concentrations, which approach ~10⁻⁵ vmr in run 5. Runs 2, 6 and 7 all featured rather abundant CH₄ compared with the modern day control run 1. The increases arose because such runs featured less OH - the main sink for CH₄ - by up to about a factor (2-3) compared with the modern Earth OH value run 1. Less OH was associated with the lowering in O₂ and with a colder, drier atmosphere in run 2 (Table 3), since OH is produced via H₂O+O(¹D)→2OH. The run with enhanced N₂O, yielding a decrease in CH₄, due to a doubling in tropospheric OH (near 10km) than the Proterozoic reference run 2, associated with the fast reaction: NO (via N₂O decomposition) + HO₂→NO₂+OH.

3.3.2 Temperature

Stratosphere – the Proterozoic runs exhibited a cooling response (Figure 3b) of up to 50K in the stratosphere, related to the lowering in O₃, which is the main heater in this region. As a result, for most runs the temperature inversion at about 0.1 bar is generally weakened compared with the control run 1, and the stratosphere shrinks in the vertical, with the stratopause moving down from about 0.001 bar (in the modern Earth run) to about 0.005 bar (in the Proterozoic runs). Runs 4 (enhanced N₂O) and run 6 (enhanced CH₃Cl) which destroyed O₃ locally in the lower- and upper-stratosphere respectively, featured enhanced cooling in these regions.

Troposphere – a fainter solar luminosity in the 10% PAL O₂ scenario (run 2) led to a reduced surface temperature of 282K compared with 288K in the modern Earth control run 1. Of the Proterozoic runs, the scenario with increased N₂O featured the warmest surface temperature (T_o=285K), whereas the other runs featured only small deviations, with all values in the range T_o=(281-282)K.

3.4 Strong lightning activity as a false positive for life?

In Table 3, increased lightning (run 3) leads to an enhancement in the biomarker O₃ compared with the Proterozoic control case (run 2). Does lightning act as a “false positive” by “artificially” increasing the biomarker signal? An investigation of this O₃ increase revealed that lightning produced some extra NO_x which yielded some smog O₃ formation i.e. strengthened the O₃ biomarker, therefore more UV-shielding. For a planet without life, hence probably with very low O₂, these responses would not occur, because the smog mechanism requires O₂ to form O₃ via $O_2+O+M \rightarrow O_3+M$. Lightning therefore, according to our results, is not a false positive but a favourable phenomenon, which enhances but does not mimic atmospheric life signals.

3.5 Theoretical Emission Spectra

We calculated spectra for the mid-infrared (IR) region (2-20) μm using the SQuIRRL model described in section 2.2 at a spectral resolution, $R = 100$. Figure 4 compares the spectral region from (2.0 to 20) μm for the modern Earth control run 1 and the Proterozoic control run 2. The well-known fundamental bands for H_2O (6.3 μm), O_3 (9.6 μm) and CH_4 (3.3 μm), are all captured in Figure 4. The CO_2 emission feature near 15 μm which indicates the atmospheric temperature inversion at the tropopause is observable only for the modern run, not for the Proterozoic run, where the inversion is weaker.

Figure 5 is as for Figure 4 but shows the “Canfield ocean” run with 100 times more N_2O emissions. In this case, some of the N_2O bands - especially the feature at 7.8 μm - are clearly enhanced. Further testing has shown that the majority of absorption from these bands arose at an atmospheric height below about 10km in the troposphere.

Des Marais et al. (2002) and Traub and Jucks (2002) investigated the effect of increasing N_2O in a theoretical spectral model and discussed under which conditions detections becomes possible. However, their imposed concentration changes were arbitrary. **The new contribution of our work is to model consistently N_2O chemical concentrations based on indications of enhanced biogenic fluxes during the Proterozoic. Our result provides an example – based on our own planet – that N_2O could be a potentially important biomarker. We remind however, that our study uses a cloud-free model, neglecting their influence on atmospheric spectra of Earth-like exoplanets (see e.g. Tinetti et al., 2006 and Kaltenegger et al., 2007).**

4. Discussion and Conclusions

This work has presented a scenario based on Proterozoic Earth, namely with a Canfield ocean having high N_2O emissions. Results suggest that N_2O may be a more important biomarker than previously thought. Also, since N_2O is an efficient greenhouse

gas, this led to about 3.5K surface warming for a Canfield ocean scenario with one hundred times enhanced N₂O surface emissions (run 4).

We have also presented a mechanism which suggests that O₃ can survive variations in source gas emissions for the Proterozoic at 10% PAL O₂. Feedbacks between N₂O, O₃ and UV imply that the O₃ column is expected to survive even high levels of N₂O emissions from Canfield ocean scenarios, and its fundamental band is mostly unchanged in the emission spectrum. Therefore, O₃ is concluded to be a good biomarker for the Proterozoic period.

Acknowledgements

We are grateful to James Kasting and to Antigona Segura for providing the initial code and for useful discussion. We thank two anonymous referees for their helpful comments. This research has been supported by the Helmholtz Gemeinschaft through the research alliance “Planetary Evolution and Life”.

References

- Bluth, G.J.S., Schnetzler, C.C., Krueger, A.J., and Walter, L.S., 1993. The contribution of explosive volcanism to global atmospheric sulphur dioxide concentrations, *Nature*, 366, 327-329.
- Buick, R., 2007. Did the Proterozoic ‘Canfield Ocean’ cause a laughing gas greenhouse? *Geobiology* 5, 2, 97-100.
- Catling, D., 2005. The story of O₂, *Science*, 308, 1730-1732.
- Catling, D., and Claire, M. W., 2005. How Earth’s atmosphere evolved to an oxic state: a status report, *Earth Pl. Sci. Lett.*, 237, 1-20.
- Catling, D., 2006. Comment on “A hydrogen-rich Early Earth atmosphere”, *Science* 311 5757 (38) 2006
- Crutzen, P.J., 1970. The influence of nitrogen oxides on the atmospheric ozone content, *Q. J. R. Meteorol. Soc.* 96, 320-325.
- Des Marais, D. J., Marwit, M., Stocks, K., Jucks, K.W., Kasting, J. F., Lin, D. N. C., Lunine, J. I., Schneider, J., Seager, S., Traub, W. A., and Woolf, N. A., 2002. Remote sensing of planetary properties and biosignatures on extrasolar terrestrial planet, *Astrobiol.* 2 1-53-181.
- Ehhalt, D. H., *Global aspects of atmospheric chemistry*, 21-110, 1999. Steinkopf Verlag, Darmstadt Germany.
- Gebauer, S., Grenfell, J. L., von Paris, P., Godolt, M., and Rauer, H., 2010. Evolution of extrasolar planetary atmospheres. I Assessing biomarkers with a global, interactive O₂-N₂-CO₂ atmospheric column model. Manuscript in preparation.
- Gough, D.O. 1981. Solar interior structure and luminosity variations, *Solar Phys.*, 74, 21-34.
- Grenfell, J.L., Stracke, B., Patzer, B., Titz, R., Rauer, H., 2006. Potential of Ozone Formation by the Smog Mechanism to shield the surface of the Early Earth from UV radiation? *Inter. J. Astrobiol.*, 5 (4), 295-306.
- Grenfell, J.L., Stracke, B., von Paris, P., Patzer, B., Titz, R., Segura, A., Rauer, H., 2007^a. The Response of Atmospheric Chemistry on Earth-like Planets around F, G and K Stars to Small Variations in Orbital Distance, *Plan.*

Spa. Sci., 55, 661-671.

Grenfell, J.L., Grießmeier, J.-M., Patzer B., Rauer, H., Segura, A., Stadelmann, A., Stracke, B., Titz, R., von Paris, P., 2007^b. Biomarker Response to Galactic Cosmic Ray-Induced NO_x and the Methane, Greenhouse Effect in the Atmosphere of an Earth-like Planet Orbiting an M-Dwarf Star, *Astrobiology*, 7, (1), 208-221.

Haagen-Smit, A.J. 1951. Chemistry and physiology of Los Angeles Smog, *Indust. Eng. Chem.*, 44, 1342-1346.

Holland, H. D., 2002. Volcanic gases, black smokers, and the great oxidation event, *Geochemica et Cosmochemica acta*, 66, 3811-3826.

Ingersoll, A.P., 1969. The runaway greenhouse: a history of water on Venus, *J. Atm. Sci.*, 26, 1191-1198.

International Panel on Climate Change (IPCC), *Climate Change 2001. The Scientific Basis*, Houghton, J.T., (ed), Cambridge University Press.

International Panel on Climate Change (IPCC), *Third Assessment Report (TAR) 2007: The Physical Science Basis*, Solomon, S., Qin, D., Manning, M., Chen, Z., Marquis, M., Averyt, K. B., Tignor, M., and Miller, H. L., Cambridge University Press and New York Press.

Kaltenegger, L., Traub, W. A., and Jucks, K. W., Spectral evolution of an Earth-like planet, *Astrophys. J.*, 658, 598-616, 2007.

Kaminski, J. W., Neary, L., Struzeska, J., McConnell, J. C., Lupu, A., Jarosz, J., Toyota, K., Gong, S. L., Cote, J., Liu, X., Chance, K., and Richter, A., 2008. GEM-AQ, an online global multiscale chemical weather modelling system, *Atmos. Chem. Phys.* 8 3255-3281.

Kasting, J. F., Pollack, J. B., and Crisp, D., 1984. Effect of high CO₂ levels on surface temperature and atmospheric oxidation state on the Early Earth, *J. Atmos. Chem.*, 1, 403-428.

Kasting, J. F., Zahnle, K. J., Pinto, J. P., and Young, A. T., 1989. Sulfur, ultraviolet radiation and the early evolution of life, *Origins of Life*, 19, 95-108.

Keppeler, F., Harper, D. B., Röckmann, T., Moore, R. M., and Hamilton, J. T.G., 2005. New insight into the atmospheric chloromethane budget gained using stable carbon isotope ratios, *Atmos. Chem. Phys.*, 5, 2403-2411.

Kitzmann, D., Patzer, A.B.C., von Paris, P., Godolt, M., Stracke B., Gebauer, S., Grenfell, J. L., and Rauer, H., 2010. Clouds in the atmospheres of extrasolar planets. Climatic effects of multi-layered clouds for Earth-like planets and implications for habitable zones, *Astron. Astrophys.*, 511, doi 10.1051/0004-6361/200913491.

Kourtidis, K., Kelesis, A., and Petrakakis, M., 2008. Hydrogen sulfide (H₂S) in urban ambient air, *Atm. Env.* 42, 7476-7482.

Lopez-Santiago, J., Micela, G., Sciortino, S., and Favata, F., 2004. Young stellar populations in the solar neighbourhood, *Mem. Soc. Astron. Italiana*, 1, 1.

Kump, L. R., Kasting, J. F., and Barley, M. E., 2000. Rise of atmospheric oxygen and the upside-down Archaean mantle, 2001. *Geochem. Geophys. Geosystems*, 2(1), 1025, doi 10.1029/2000GC000114.

Manabe, S. and Wetherald, R., 1967, Thermal Equilibrium of the Atmosphere with a Given Distribution of Relative Humidity, *Journal of Atmospheric Sciences*, vol. 24, Issue 3, pp.241-259.

Meadows, V., and Crisp, D., 1996. Ground-based near infra-red measurements of Venus nightside: the thermal structure and water abundance near the surface, *J. Geophys. Res.*, 101, 4595-4622.

Melsheimer, C., Verdes, C., Buehler, S. A., Emde, C., Eriksson, P., Feist, D. G., Ichizawa, S., John, V. O., Kasai, Y., Kop, G., Koulev, N., Kuhn, T., Lemke, O., Ochiai, S., Schreier, F., Sreerrekha, T. R., Suzaki, M., Takahashi, C., Tsujimaru, S., and Urban, J., 2005. Intercomparison of general purpose clear sky atmospheric radiative transfer models for the m

Mlawer, E.J., Taubman, S.J., Brown, P.D., Iacono, M.J., Clough, S.A, 1997. Radiative transfer for inhomogeneous atmospheres: RRTM, a validated correlated-k model of the longwave, *J. Geophys. Res.*, 102, 16,663-16,682.

Mvondo, D.N., Navarro-González, R., McKay, C. P., Coll, P., Raulin, F., 2001. Production of nitrogen oxides by lightning and coronae discharge in simulated early Earth, Venus and Mars environments, *Adv. Space. Res.*, 27, 2, 217-223.

- Navarro-González, R., Molina, M.J., Molina, L.T., 1998. Nitrogen fixation by volcanic lightning in the early Earth, *Geophys. Res. Lett.*, 25, 3123–3126.
- Pavlov, A. A., Kasting, J. F., Brown, L. L., Rages, K. A., and Freedman, R., 2000. Greenhouse warming by CH₄ in the atmosphere of early Earth, *J. Geophys. Res.*, 105, 11,982-11,990.
- Pavlov, A. P., Hurtgen, M. T., Kasting, J. F., and Arthur, M. A., 2003. Methane-rich Proterozoic atmosphere? *Geology*, 31, 87-90.
- Rauer, H., Gebauer, S., von Paris, P., Cabrera, J., Godolt, M., Grenfell, J. L., Belu, A., Selsis, F., and Hedelt, P., 2010 (submitted). Biomarkers in Super-Earth atmospheres I. Spectral appearance of Super-Earths around M-stars.
- Ribas, I., Guinan, E. F., Güdel, M., and Audard, M., 2005. Evolution of the solar activity over time and effects on planetary atmospheres. I. High-energy irradiances (1-1700 Angstrom), *Astrophys. J.* 622, 680-694.
- Rothman, L.S., Jacquemart, D., Barbe, A., Benner, D.C., Birk, M., Brown, L.R., Carleer, M.R., Chackerian, C., Chance, K., Coudert, L. H., Dana, V., Devi, M., Flaud, J.M., Gamache, R.R., Goldman, A.A., Hartmann, J.M., Jucks, K.W., Maki, A., Mandin, J.Y., Massie, S.T., Orphal, J., Perrin, A., Rinsland, C.P., Smith, M.A.H., Tennyson, J., Tolchenov, R.N., Toth, R.A., Vander, A., Auwera, J., Varanasi, P., and Wagner, G., 2005. The HITRAN 2004 molecular spectroscopic database, *Spectrosc. Radiat. Transfer*, 96 (2), 139-204.
- Schindler, T. L., and Kasting, J. F., 2000. Synthetic spectra of simulated terrestrial atmospheres containing possible biomaterial gases, *Icarus*, 145, 262-271.
- Schreier, F., and Böttger, U., 2003. MIRART, a line-by-line code for infrared atmospheric radiation computations including derivatives. *Atmos. Oceanic Opt.*, 16(3), 262-268.
- Segura, A., Krelove, K., Kasting, J.F., Sommerlatt, D., Meadows, V., Crisp, D., Cohen, M., Mlawer, E., 2003. Ozone concentrations and ultraviolet fluxes on Earth-like planets around other stars, *Astrobiology*, 3 (4), 689-708.
- Selsis, F., D. Despois, and J. –P. Parisot, 2002. Signatures of life on exoplanets: can Darwin produce false positive detections? *Astron. Astrophys.*, 388, 985-1003.
- Shields, F., and J. F. Kasting, Paleoclimatology: evidence for hot early oceans, *Nature* 447, 10.10138/nature0530, 2007.
- Tian, F., Toon, O., Pavlov, A., and De Sterck, H., (2005), A hydrogen-rich Early Earth atmosphere, *Science* 308, 1014-1017.
- Tinetti, G., Meadows, V. S., Crisp, D., Kiang, N. Y., Kahn, B. H., Fishbein, E., Velusamy, T., and Turnbull, M., Detectability of planetary characteristics in disk-averaged spectra II: synthetic spectra and lightcurves of Earth, *Astrobiol.*, 6 (6), 881-900, 2006.
- Toon, O.B., McKay, C.P., Ackerman, T.P., Santhanam, K., 1989. Rapid calculation of radiative heating rates and photodissociation rates in inhomogeneous multiple scattering atmospheres, *Journal of Geophysical Research*, 94, 16,287-16,301.
- Traub, W. A., and Jucks, K. W., A possible aeronomy of extrasolar terrestrial planets, AGU monograph series v. 130, "Atmospheres in the solar system: Comparative aeronomy", ed., Mendillo, M., Nagy, A., and Waite, J. H., 369-380, 2002.
- World Meteorological Organisation, (WMO) Scientific Assessment Of Ozone Depletion 1994, 1995. Global ozone research and monitoring project report No.37, Geneva.

Tables

Table 1: Comparison of total surface emission fluxes (Tg (10^{12} g)/year) for observations, the modern-day control run by Segura et al. (2003) and for our modern control run. Values in brackets represent the natural (without manmade) component only. Negative values for H_2 imply loss from the atmosphere which corresponds to a net H_2 deposition velocity of $7.7 \times 10^{-4} \text{ cm s}^{-1}$.

Scenario	CH ₄	N ₂ O	CH ₃ Cl	H ₂	CO	lightning NO	SO ₂	H ₂ S
Observations Modern Earth	500 to 600# (150- 270)*	6.7 to 36.6# (4.6- 16.8)	2.9# (2.7)	-3* Ehhalt (1999)	1060 (TAR 2007)	12.2 Kaminski et al. (2008)	(2-50) Bluth et al. (1993)	>2.6 Kourtidis et al. (2008) ^{###} (uncertain)
Segura et al. (2003) control	954	13.2	7.3	-1.3	2350	Not quoted	58	3.3
This work Control (run 1)	531	4.3	3.4	-5.5	1800	10.5	58	3.3

*Difficult to separate natural from manmade sources. #Taken from International Panel on Climate Change (IPCC 2001), IPCC TAR (2007) and references therein. ^{###} sum of manmade traffic emissions for Europe and Asia.

Table 2: Overview of the various calculation scenarios. “Faint sun” denotes the factor by which the top of atmosphere incoming solar radiation flux is reduced compared with its modern value. “PAL” denotes Present Atmospheric Level. “Tg/year” denotes surface emissions in Tg/year. CO₂ was set to 355ppm in the control run and to a pre-industrial value of 277ppm in the other runs. All runs were calculated with an adjusted surface albedo of 0.21. *Negative H₂ values indicate net removal at the surface with a constant dry deposition velocity (see text), proportional to the H₂ concentration in the atmosphere, except in run 7 (high H₂ run) where a positive, constant, surface flux was prescribed.

Run	Scenario	Faint Sun Factor	% PAL O ₂	CH ₄ surface (Tg/yr)	CH ₃ Cl surface (Tg/yr)	N ₂ O surface (Tg/yr)	NO lightning (Tg/yr)	H ₂ * surface (Tg/yr)
1	Modern Control	1	100	531	3.4	4.3	10.5	-5.5
2	10% O ₂ Control	0.943	10	531	3.4	4.3	10.5	-11.4
3	10% O ₂ x10 lightning	0.943	10	531	3.4	4.3	105.0	-5.0
4	10% O ₂ x100 N ₂ O	0.943	10	531	3.4	430	10.5	-4.5
5	10% O ₂ x2 CH ₄	0.943	10	1062	3.4	4.3	10.5	-25.3
6	10% O ₂ x10 CH ₃ Cl	0.943	10	531	34.0	4.3	10.5	-7.1
7	10% O ₂ high H ₂	0.943	10	531	3.4	4.3	10.5	+25.0

Table 3: Column densities (Dobson Units) of atmospheric species investigated.

Run	Scenario	O ₃	N ₂ O	CH ₄	CH ₃ Cl	H ₂ O
1	Modern Control	305	233	1240	0.4	2.4x10 ⁶
2	10%PAL O ₂ control	269	77	3260	1.0	1.4x10 ⁶
3	10%PAL O ₂ x10 lightning	287	77	1185	0.3	1.4x10 ⁶
4	10%PAL O ₂ x100 N ₂ O	183	3924	1094	0.3	1.9x10 ⁶
5	10%PAL O ₂ x2 CH ₄	264	75	7987	1.2	1.6x10 ⁶
6	10%PAL O ₂ x10 CH ₃ Cl	159	33	1670	4.9	1.4x10 ⁶
7	10%PAL O ₂ high H ₂	266	75	3447	1.0	1.5x10 ⁶

Table 4: Quantities relevant to the modeled N₂O budget. Rates of atmospheric N₂O sinks are output at 20km. Shown are chemical reaction rates (molecules cm⁻³ s⁻¹) and column values (Dobson Units) integrated over the complete model atmosphere. Atmospheric (inorganic) sources are negligible and are not shown.

Quantity	Modern Earth (run 1)	10% PAL O ₂ (run 2)
Rate N ₂ O+hv	43.9	616.2
Rate N ₂ O+O ¹ D	44.6	21.1
O ₃ column (DU)	305	269
N ₂ O column (DU)	233	77

Figure Captions

Figure 1a: Atmospheric ozone (O_3) profiles. Key: Solid = modern-day control (run 1). Long-Dashed = 10% PAL O_2 control (run 2). Short-dashed = 10% PAL O_2 x10 lightning (run 3). Long-short dashed = 10% PAL O_2 x100 N_2O (run 4). Dots = 10% PAL O_2 x2 CH_4 (run 5). Dot-dashed = 10% PAL O_2 x10 CH_3Cl (run 6). Dot-dot dashed = 10% PAL O_2 x10 H_2 (run 7).

Figure 1b: As for Figure 1a but for nitrous oxide (N_2O).

Figure 2a: Processes related to ozone-nitrous oxide feedbacks. Y-axis shows atmospheric column amounts in Dobson Units (DU) and UV-B radiation (Wm^{-2}) in the upper troposphere (16km). X-axis shows the factor by which the surface N_2O emissions (E_{N_2O}) are increased relative to the modern day control run (modern $E_{N_2O} = 4.3$ Tg N_2O /year, Table 1).

Figure 2b : Response of ozone photochemistry near 10km to changes in the surface N_2O flux. “%smog” denotes the amount of ozone formed from the smog mechanism ($O_{3(smog)}$), “%Chapman” denotes the amount of ozone formed from the Chapman cycle ($O_{3(Chapman)}$) i.e. Chapman only, without catalytic loss cycles. These two quantities are based upon straightforward steady-state equations which assume NO_2 and O^3P (calculated from the model) are in chemical balance.

Figure 3a: Atmospheric methane (CH_4) profiles. Key as for Figure 1.

Figure 3b: Atmospheric temperature (Kelvin) profiles. Key as for Figure 1.

Figure 4: Theoretical spectrum with resolution, $R (= \lambda/\Delta\lambda) = 100$, for modern Earth control run 1 and the Proterozoic reference run 2 for the (2-20) micron range.

Figure 5: As for Figure 4 but for modern Earth control run 1 and the Proterozoic run with x100 enhanced N_2O run 4.

Figure 1a Ozone abundance

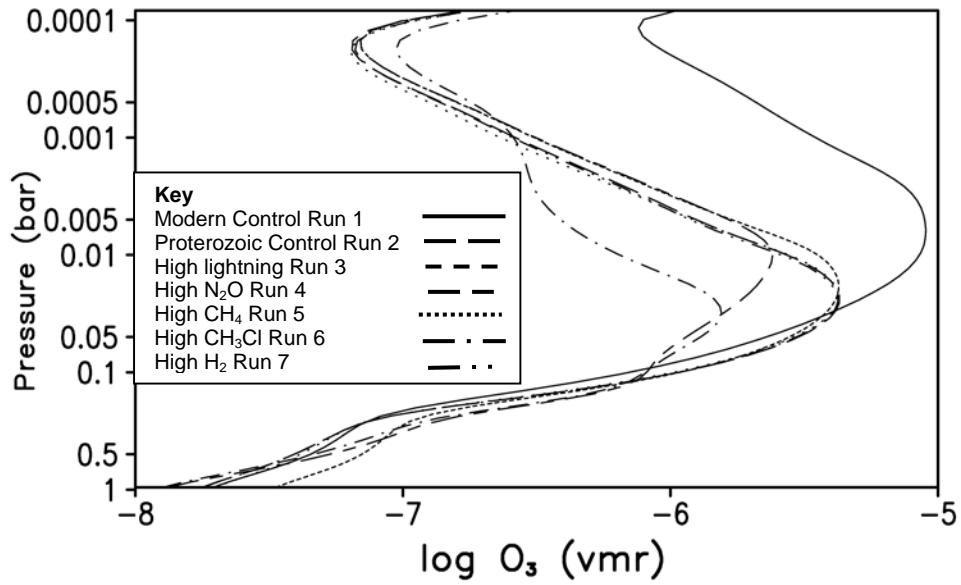


Figure 1b Nitrous oxide abundance

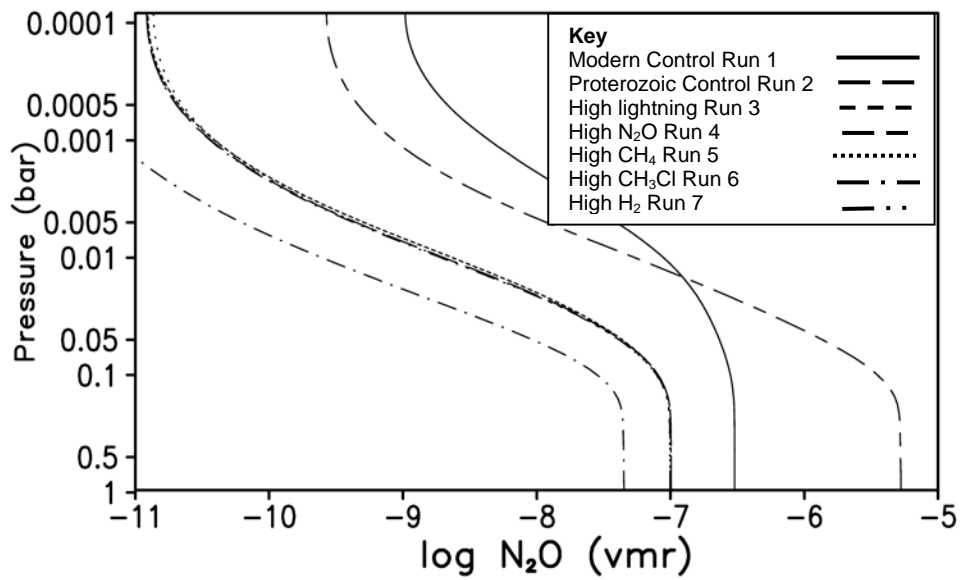
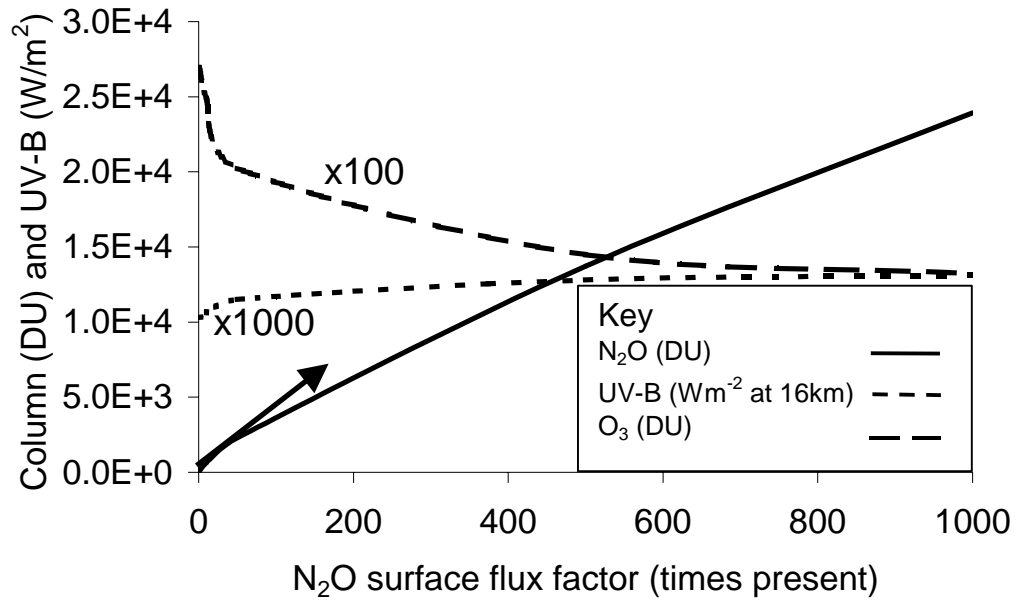


Figure 2a N₂O and O₃ feedbacks



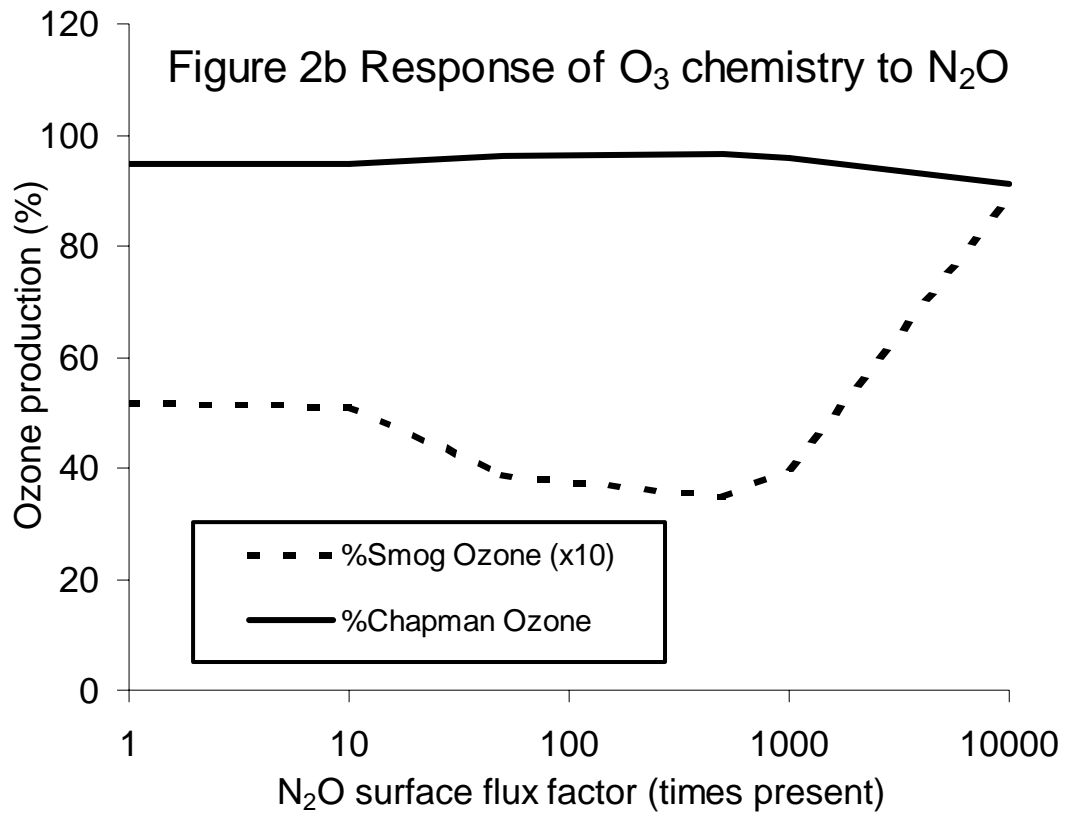


Figure 3a Methane abundance

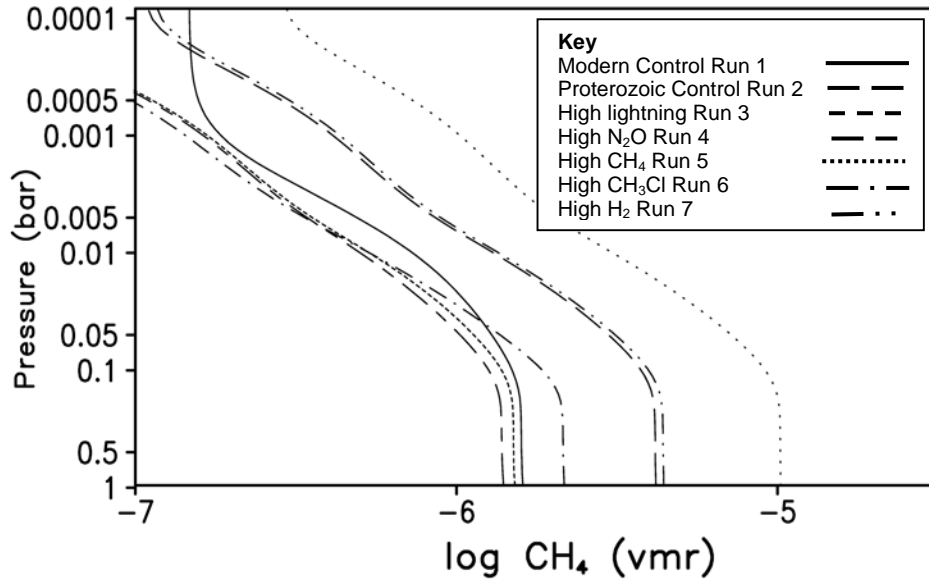


Figure 3b Temperature

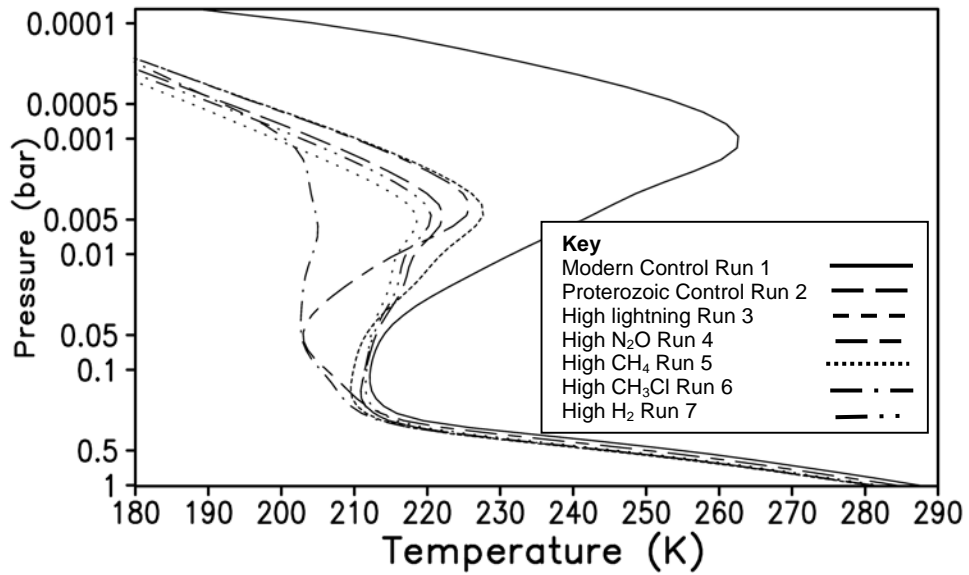


Figure 4: Synthetic spectra (R=100)

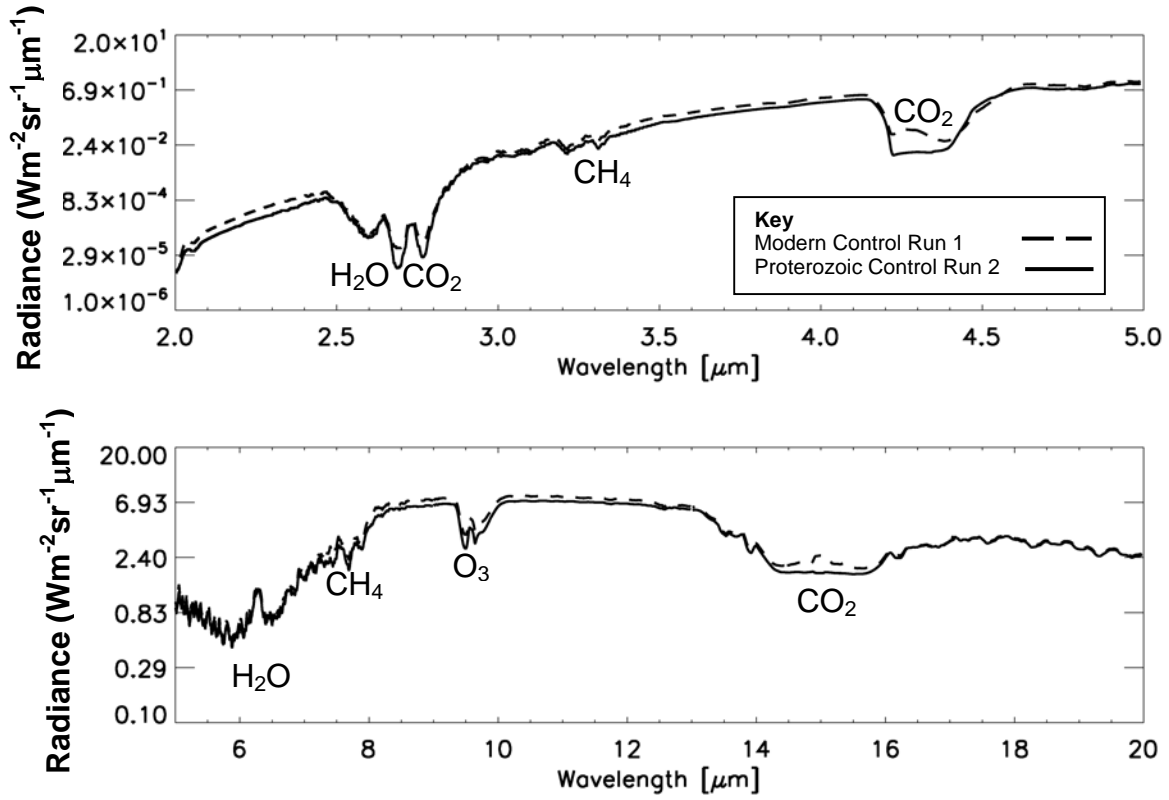


Figure 5 Synthetic spectra (R=100)

